Journal of Materials Chemistry A

PAPER

View Article Online
View Journal | View Issue

Cite this: J. Mater. Chem. A, 2017, 5, 10470

Hyperbranched poly(ether amine)@poly(vinylidene fluoride) (hPEA@PVDF) porous membranes for selective adsorption and molecular filtration of hydrophilic dyes†

Kejia Ji, Hongjie Xu, Xiaodong Ma, Jie Yin and Xuesong Jiang *

Porous membranes with selective adsorption are of great interest because of their wide application in molecular filtration, industrial separation and water treatment. To adsorb dyes with selectivity and high flux, the unique selective adsorption behavior of amphiphilic hyperbranched poly(ether amine) (hPEA) materials toward guest molecules and the facile preparation of a stable porous structure of poly(vinylidene fluoride) (PVDF) were combined to fabricate novel hPEA@PVDF porous membranes through non-solvent induced phase separation (NIPS). The resulting hPEA@PVDF membranes were further cross-linked through the photo-dimerization of coumarin groups in hPEA, and their morphologies were characterized using a scanning electron microscope (SEM), wide angle X-ray diffractometer (WAXD) and differential scanning calorimeter (DSC). The adsorption behavior of hPEA@PVDF porous membranes toward twelve hydrophilic dyes was investigated in detail. Regardless of their charge states, hPEA@PVDF porous membranes exhibited quick adsorption behavior toward Erythrosin B (ETB), Rose Bengal (RB) and Eosin B (EB) with a high adsorption capacity (Q_{eq}) around 600 μmol g^{-1} but very slow adsorption behavior toward Calcein (Cal) and Methylene Blue Trihydrate (MB) with a low adsorption capacity. Based on their unique selective adsorption behavior toward hydrophilic dyes, hPEA@PVDF porous membranes could separate mixtures of dyes in aqueous solution through molecular filtration with a high flux rate. In addition, the hPEA@PVDF porous membranes were easily regenerated and maintained high separation efficiency over five adsorption–washing cycles. hPEA@PVDF membranes showed great advantages of large adsorption capacity, fast separation of dyes, easy regeneration and low cost due to their porous structure and unique selective adsorption behavior toward hydrophilic dyes, and might find great potential in separation and water treatment.

Received 11th March 2017
Accepted 25th April 2017

DOI: 10.1039/c7ta02176c

rsc.li/materials-a

1. Introduction

Porous materials with unique characteristics such as high surface area, large accessible space and interconnected hierarchical porosity[1] can be applied for separation through membrane filtration.[2,3] As an emerging area of great interest in separation, molecular filtration is based on the membrane's high selectivity, which is the key factor to filter molecules with a high flux. The selectivity is dependent on the chemical features of the membrane, and provides the possibility for the membrane to separate mixtures with molecules of nearly the same size through molecular filtration, which makes the membranes very promising in the fields such as water treatment,[4–8] gas separation,[9–11] purifying drug molecules and biomolecules,[12] detecting drugs[13] and organics recycling.[14,15] Therefore, membranes with both high selectivity for guest molecules and high flux[16] will be of great potential for molecular filtration.[17–20]

As one of the most important porous membranes, poly(vinylidene fluoride) (PVDF) membranes with an asymmetric structure[21,22] are ideal to obtain high permeability due to their high porosity and appropriate pore structure. Furthermore, PVDF porous membranes show outstanding properties such as high mechanical strength, thermal stability, chemical resistance and well-controlled porosity.[23,24] Thus, PVDF membranes are widely used in filtration processes for separation through various modifications, in which most of these filtration processes are mainly physical sieving controlled by channel sizes.[21,25–27] Due to the hydrophobic nature of PVDF, however, the application of pure PVDF membranes in water treatment is limited because water flux through PVDF is usually low[28] and PVDF is susceptible to fouling when exposed to polluted water.[29,30] To extend the application of PVDF in water treatment,

School of Chemistry & Chemical Engineering, State Key Laboratory for Metal Matrix Composite Materials, Shanghai Jiao Tong University, Shanghai 200240, People's Republic of China. E-mail: ponygle@sjtu.edu.cn

† Electronic supplementary information (ESI) available. See DOI: 10.1039/c7ta02176c

it is significant to improve the hydrophilicity of PVDF membranes to increase the water flux and resist fouling, and consequently reduce the operation cost. Usually, combining various material types to obtain new membranes could favor the new membranes with enhanced functional and mechanical properties.[31] Blending hydrophilic polymers[32,33] or amphiphilic copolymers[34–36] with PVDF is the most practical and efficient way to enhance the hydrophilicity of PVDF membranes. Lü[37] reported that by blending hydrophilic polyurethane with PVDF, the permeability and anti-fouling performance of PVDF were improved. Rajasekhar[38] blended amphiphilic triblock copolymers and PVDF to fabricate ultrafiltration membranes, which can be used for the separation of oil–water emulsion. Blending hydrophilic polymers or amphiphilic copolymers not only enhances the hydrophilicity of PVDF membranes to increase the water flux, but also provides the possibility to control the transport properties of the membranes.

Recently, we developed a novel type of hydrogel based on amphiphilic hyperbranched poly(ether amine) (hPEA), which showed unique selective adsorption behavior toward hydrophilic dyes in aqueous solution, and could be used in the separation and removal of dyes in water treatment through static adsorption.[39,40] The investigation revealed that the hydrophobic–hydrophilic interaction between hPEA-based hydrogels[41] and hydrophilic dyes may lead to selective adsorption properties.

As is well known, most organic dyes have complex aromatic molecular structures that make them stable and difficult to biodegrade,[42] especially synthetic dyes. The extensive use of dyes often causes serious pollution, and for some dyes, a concentration of less than 1 ppm can color large water volumes, which may potentially be toxic or mutagenic and carcinogenic for biological diversity.[43] To combine the characteristics of the selective adsorption capacity of amphiphilic hPEA and the porous structure of PVDF, we here fabricated a type of hPEA@PVDF hybrid porous membrane through the NIPS process, in which the porous skeleton of PVDF was covered by the cross-linked layer of the hPEA hydrogel (Scheme 1). During the process of removing dyes in water treatment, the hPEA@PVDF hybrid porous membranes could separate the dye mixture simultaneously through molecular filtration. The porous skeleton of PVDF provided a mechanically and chemically stable support for the hPEA hydrogel, providing a large surface area for adsorption. The cross-linked layer of the hPEA hydrogel could not only allow selective adsorption of dyes to realize molecular filtration, but also enhance the hydrophilicity of the PVDF porous skeleton to increase the water flux in the process of filtration. Therefore, it was the synergistic effect of the hPEA hydrogel and PVDF porous skeleton that makes it possible for the hPEA@PVDF membrane to separate dyes through molecular filtration. Compared with our previous work on hPEA-based nanoparticles and hydrogels, porous hPEA@PVDF membranes could be prepared through the one-pot and NIPS methods, which were economical and facile. Besides, hPEA@PVDF membranes could adsorb dyes *via* molecular filtration with a higher flux, larger adsorption capacity and faster adsorption rate than static adsorption.

2. Experimental section

2.1 Fabrication of hPEA@PVDF membranes

The amphiphilic copolymers hPEA-EC-CF6 were synthesized by introducing epoxy-containing coumarin moieties (EC) and fluorinated carbon chains (CF6) into the periphery of hPEA through epoxy/amine click chemistry. The detailed synthesis is shown in ESI 1.2 & 2.1.† The membranes were fabricated *via* the NIPS method. The blend solutions were prepared by dissolving PVDF and hPEA-EC-CF6 in DMAc for 24 h at 60 °C to obtain a homogenous casting solution; the ratios of the blends are listed in Table 1. And the standing time of the casting solutions was at least 12 hours to eliminate internal bubbles. The casting solutions were then cast onto a glass plate at 20 °C using a self-made scraper to produce a flat sheet membrane. After that, the casting solution along with the glass plate was immersed in a 20 °C de-ionized water bath for 10 minutes to leach the solvent out. Then the membranes were taken out of the water bath and kept in de-ionized water for 3 days to ensure the full exchange of water and DMAc. After they were taken out of de-ionized water,

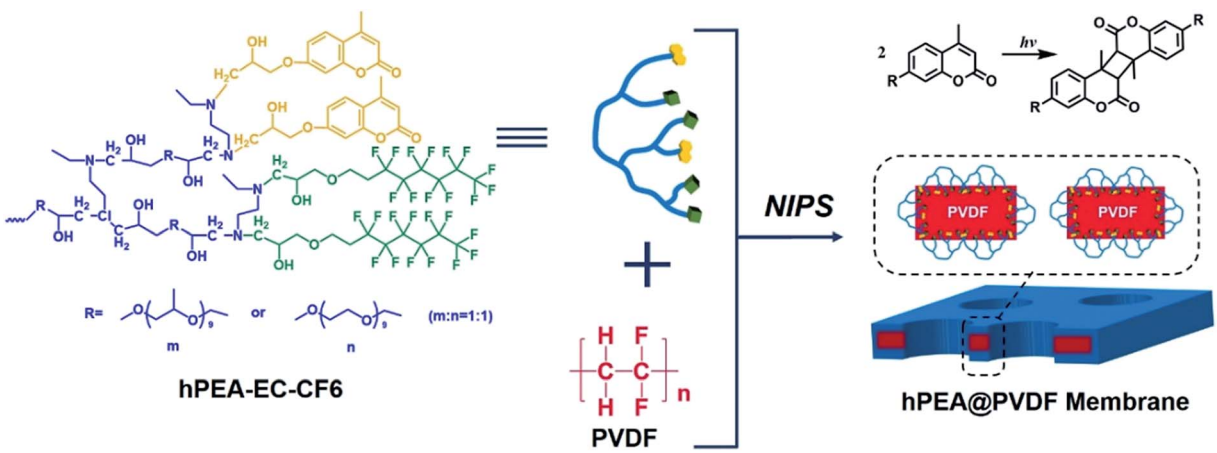

Scheme 1 Chemical structure of amphiphilic hPEA and the strategy for the fabrication of hPEA@PVDF porous membranes through NIPS.

Table 1 Composition of hPEA@PVDF membranes and water contact angles on their surfaces

Sample	PVDF [wt%]	hPEA [wt%]	Contact angle [°]
PVDF	10.0	0.00	75.2
P10@hPEA2.5	10.0	2.50	<10.0
P10@hPEA3.3	10.0	3.33	<10.0
P10@hPEA5.0	10.0	5.00	<10.0
P10@hPEA10	10.0	10.0	<10.0
P15@hPEA5.0	15.0	5.00	<10.0

the wet membranes were dried in air at room temperature, and were exposed to UV irradiation at 365 nm for 10 h. Owing to the photodimerization of the coumarin moieties, the entire hPEA@PVDF membranes were photo-crosslinked. The series of membranes were named Px@hPEAy. Here, x and y represent the concentration of PVDF and hPEA in the casting solution, respectively.

2.2 Pure water flux tests

To evaluate the membrane permeability, pure water permeation tests were conducted using a dead-end filtration cell. hPEA@PVDF membranes were tested directly at 1 bar without any pre-treatment, as the membranes could maintain high flux without flux decline. On the other hand, pure PVDF membranes were tested at a pressure of 2 bar for 30 min before testing at 1 bar. The steady pure water flux is presented below:

$$J = \frac{V}{A \times t} \quad (1)$$

where J (L m^{-2} h^{-1}) is the water flux, V (L) is the pure water volume, A (m^2) is the effective membrane area, and t (h) is the time of permeate collection.

2.3 Adsorption experiments

Twelve hydrophilic dyes were chosen for the adsorption experiments, and their structures are shown in Fig. S6.† The dye concentration was traced by measurements at the maximum absorption wavelength using a UV-vis spectrophotometer.

In saturated adsorption experiments, fluorescein dyes were dissolved in buffered aqueous media at pH 7.2, and azo dyes and MB were dissolved in deionized water. The adsorbent (15 mg) was immersed in dye solution (C = 300 μmol L^{-1} volume = 15 mL). After 48 h at 25 °C, the equilibrium adsorption capacity (Q_{eq}) of the dyes was tested. Q_{eq} is defined as follows:

$$Q_{eq} = \frac{C_0 - C_{eq}}{M} V \quad (2)$$

where Q_{eq} (μmol g^{-1}) is the amount of adsorbed dyes per gram of adsorbent at equilibrium; C_0 is the initial concentration of dyes in the solution (μmol L^{-1}); C_{eq} is the concentration of dyes at equilibrium (μmol L^{-1}); V is the volume of the solution (L), and M is the mass of the adsorbent used (g).

For the adsorption kinetics tests, the P15@hPEA5.0 membrane (30 mg) was added to the dye solution. The initial concentration of all dyes was 40 μmol L^{-1}. Concentrations varying over time were recorded. For the adsorption isotherm tests, the P15@hPEA5.0 membrane (10 mg) was immersed in dye solutions with various concentrations. These samples were kept at 25 °C for 48 hours for equilibrium.

2.4 Molecular filtration of a sole dye through a hPEA@PVDF membrane

The experiment was conducted with the general silica sand filtration unit. A vacuum pump was used to control the flow rate of dye filtration to be 10 mL min^{-1}. To trace the concentration of the dye before and after the filtration, UV-vis spectra were applied. In the experiment, the dye buffer solution (C = 40 μmol L^{-1}, pH = 7.2) was filtered through a piece of P15@hPEA5.0 membrane (diameter = 4 cm, mass = 110 mg). UV-vis spectra were recorded to trace the dye concentration of the filtrate at different filtration volumes until the concentration remained steady. The breakthrough curves of the dye through the P15@hPEA5.0 membrane could be obtained by analyzing the UV-vis spectra.

2.5 Molecular filtration of mixed dyes through a hPEA@PVDF membrane

The mixed dye solutions of ETB/MB (volume = 100 mL) and RB/Cal (volume = 100 mL) were prepared. The concentration of the dyes in the mixed solution was 20 μmol L^{-1}. To further confirm the separation capacity of the hPEA@PVDF membrane, a more complex mixed dye solution of ETB/EB/RB/Cal (volume = 50 mL) was prepared. In this solution, the concentration of each dye was 10 μmol L^{-1}. These mixed solutions were filtered through the P15@hPEA5.0 membrane (diameter = 4 cm, mass = 110 mg) at a flow rate of 6.7 mL min^{-1}. The UV-vis spectra were recorded to analyze the concentration of the dyes before and after filtration. The process of separating ETB and MB in one solution was taken as a video with a camera.

2.6 Regeneration of hPEA@PVDF membranes

After ETB and MB were separated from the mixed solution, the P15@hPEA5.0 membrane (diameter = 4 cm, mass = 110 mg) that has the adsorbed dyes was washed with a dilute NaOH solution (5 mg mL^{-1}) to elute the dyes. After the regeneration, the mixed solution of ETB/MB described above was filtered through the membrane again. Then, the UV-vis spectra were recorded to measure the concentration of the dyes in the filtrate. The separation efficiency (η) is defined as follows:

$$\eta = \frac{[MB]_{aq}}{[MB]_{aq} + [ETB]_{aq}} \times 100\% \quad (3)$$

This cycle was repeated 5 times.

2.7 Characterization methods

^{1}H-Nuclear magnetic resonance spectroscopy (^{1}H-NMR) measurements with $CDCl_3$ as the solvent were carried out using

a Varian Mercury Plus 400 MHz spectrometer at room temperature.

Fourier transform infrared spectroscopy (FT-IR) spectra were acquired using a Paragon 1000 Fourier transformation infrared absorption spectrometer (Perkin Elmer, Inc., USA).

Diffuse reflectance ultraviolet visible spectra were recorded with a Perkin-Elmer Lambda 750S UV-vis Spectrometer. The samples at different irradiation times were prepared by sticking the hPEA@PVDF membranes onto a white paper which was used as the background. This method combined with FT-IR was used to trace the photo-crosslinking process of hPEA@PVDF membranes.

The differential scanning calorimetry (DSC) curves of hPEA@PVDF membranes and their reactants were recorded on a Pyris 1 differential scanning calorimeter (DSC, Perkin Elmer, Inc., USA).

Wide angle X-ray diffraction (WAXD) analyses were performed on a Bruker D8 Advance diffractometer with Cu Kα radiation.

The X-ray photoelectron spectra (XPS) were recorded on an AXIS ULTRA DLD (Kratos) X-ray photoelectron spectrometer.

Scanning electron microscope (SEM) images were obtained using a Sirion 200 (FEI Company) field emission scanning electron microscope operated at an acceleration voltage of 5 kV; all of the membranes were coated with gold particles for observation.

The water contact angles of the membranes were measured with a contact angle meter (model CAM Micro) at room temperature. De-ionized water was added dropwise onto the surface of the membranes at three different sites to obtain the average value of contact angles.

A TU-1901 UV-vis spectrometer (Persee, China) was employed to measure the absorbance of dyes.

3. Results and discussion

3.1 Fabrication and characterization of hPEA@PVDF membranes

Scheme 1 illustrates the whole strategy for the fabrication of hPEA@PVDF porous membranes through NIPS. The amphiphilic hPEA-EC-CF6 was comprised of hydrophilic hyperbranched poly(ether amine) (hPEA) as the backbone and hydrophobic coumarin (EC) and fluorinated carbon chains (CF6) in the periphery, and was synthesized by introducing epoxy-containing coumarin moieties and fluorinated carbon chains into the periphery of hPEA through epoxy/amine click chemistry. The detailed synthesis and characterization of hPEA-EC-CF6 are shown in ESI 1.2, 2.1, Fig. S1 and S2,† and hPEA-EC-CF6 is abbreviated as hPEA in the following experiments. The incorporation of hydrophobic CF6 rich in fluorine atoms might enhance the compatibility between hPEA and PVDF, while coumarin moieties (EC) could undergo well-known photo-dimerization to lead to a cross-linked network of the hPEA layer by irradiation with UV-light, thus enhancing the stability of hPEA@PVDF porous membranes. As shown in Scheme 1, hPEA and PVDF with different ratios were first dissolved in DMAc to form a mixture of casting solution, which was then cast onto a glass substrate. Then, the casting membranes were immersed in de-ionized water, and phase separation was initiated with the exchange of DMAc in casting membranes and water. It was expected that the amphiphilic hPEA would migrate toward the interface during phase separation, and both the hydrophobic EC and CF6 moieties would interact with PVDF due to the hydrophobic interaction. Through this way, a series of hPEA@PVDF porous membranes were prepared and are listed in Table 1.

To enhance the stability, the resulting hPEA@PVDF membranes were further cross-linked through photo-dimerization of coumarin moieties, and this process was traced by UV-vis spectra and FT-IR spectra (Fig. S3†). Taking P10@hPEA2.5 as the example, the peak ascribed to the adsorption of coumarin in UV-vis spectra decreased gradually with increasing irradiation of 365 nm UV-light, suggesting the dimerization of the coumarin moieties. As shown in FT-IR spectra, the peak of C=O in coumarin units shifted from 1721 cm^{-1} to 1731 cm^{-1}. The photo-dimerization can weaken the conjugation effect of coumarin, resulting in the increased stretching vibration energy of C=O in coumarin units. These results confirmed the occurrence of photo-dimerization of coumarin moieties in hPEA.

As expected, the amphiphilic hPEA would migrate to the interface of hPEA@PVDF membranes, thus enhancing the surface hydrophilicity of the membranes. The improvement of hydrophilicity was confirmed by water contact angle (WCA) experiments. As summarized in Table 1, the WCA of the pure PVDF membrane was 75.2° due to the hydrophobic nature of PVDF, while the WCAs of hPEA@PVDF membranes were less than 10 (Fig. S5†). When the water droplet came into contact with hPEA@PVDF membranes, it spread out too quickly on the surface to be captured, suggesting the highly hydrophilic surface of hPEA@PVDF membranes.

The morphologies of the obtained hPEA@PVDF membranes were observed by SEM with the pure PVDF membrane as reference. As shown in Fig. 1, in cross sectional images, the pristine PVDF membrane exhibited a typically asymmetric structure with finger-like pores beneath the top layer. In contrast, hPEA@PVDF membranes showed an asymmetric structure constituted by a top layer, macrovoids, and a sponge-like sublayer (shown in the magnified cross sectional images taken from where the red rectangles marked), in which the macrovoids became larger with increasing content of hPEA. The difference of the micro-structure could be caused by the addition of hPEA. When the casting membranes were immersed in water, amphiphilic hPEA would migrate toward the top layer and surface of the PVDF skeleton during the phase inversion process because of its hydrophilicity. Consequently, the total polymer concentration could be higher at the top layer than in the bottom, leading to a denser surface compared to the virgin PVDF membrane. And this point was further confirmed by the expansion of the polymer-lean phase in the bulk in the cross-sectional images of hPEA@PVDF membranes. Meanwhile, it is well understood that the addition of amphiphilic copolymers and the low polymer concentration in the casting solution would increase the membrane surface pore size. The surface images of hPEA@PVDF membranes showed

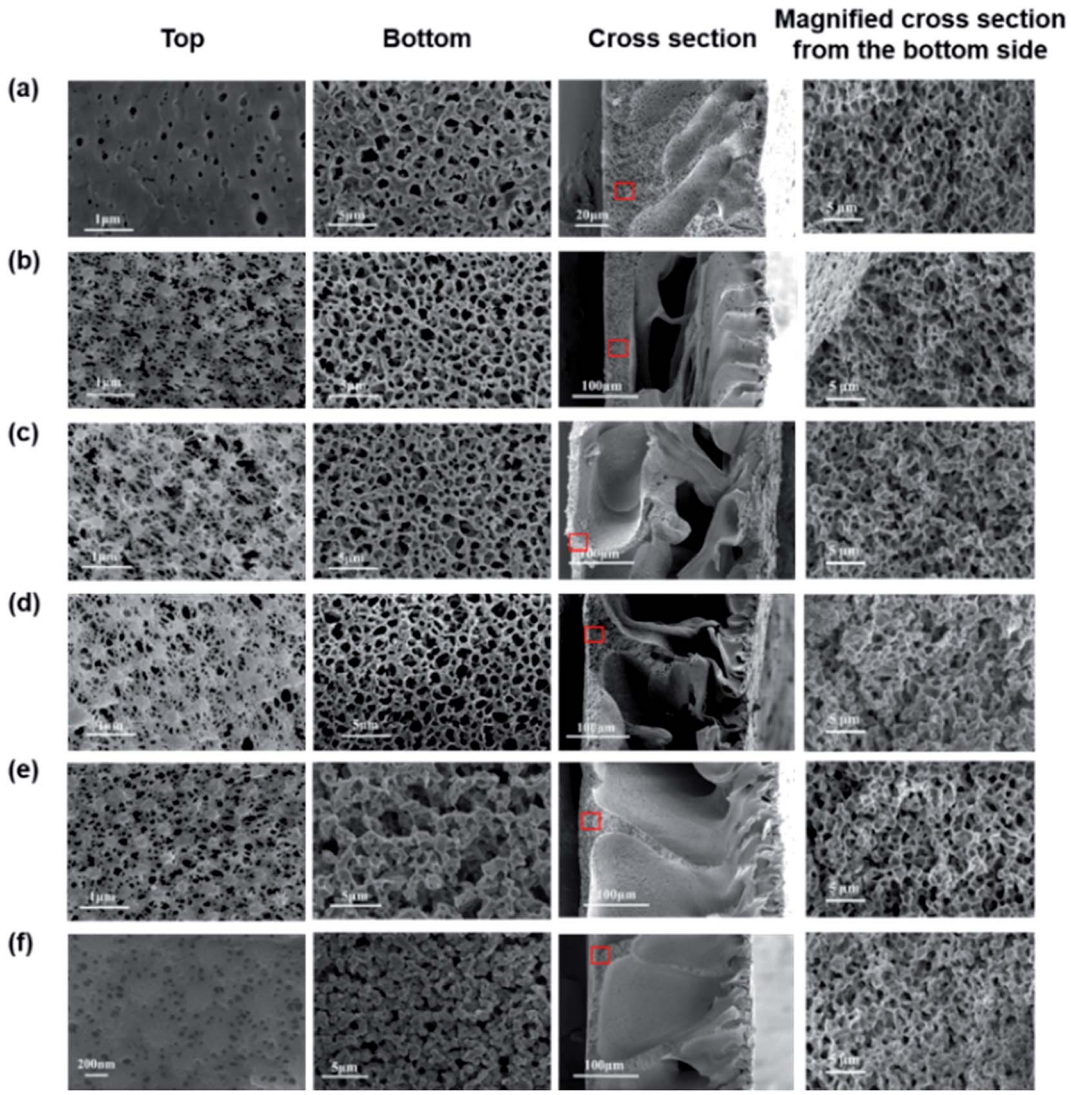

Fig. 1 SEM images of the cross-section, top surface, bottom surface and magnified cross-section from the bottom side of hPEA@PVDF membranes. Samples are (a) PVDF, (b) P10@hPEA2.5, (c) P10@hPEA3.3, (d) P10@hPEA5.0, (e) P10@hPEA10 and (f) P15@hPEA5.0.

that the pore size was larger when the membranes possessed a higher content of hPEA. Although the blend ratios of P15@hPEA5.0 and P10@hPEA3.3 were the same, P15@hPEA5.0 exhibited a smaller pore size due to its larger polymer concentration (Fig. 1e and f). From the top and bottom surface images, the pore sizes of the membranes increased in the order of P15@hPEA5, P10@hPEA2.5, P10@hPEA3.3, P10@hPEA5.0 and P10@hPEA10, and the order was consistent with the average pore size in Table S1.† It was reasonable to assume that the inflows of solvent and non-solvent were enhanced by the addition of amphiphilic hPEA, which might result in macrovoid growth. The porosity and thickness of the membranes are also summarized in Table S1.† Generally, the increase of polymer concentration makes the porosity decrease, and the addition of amphiphilic copolymers would increase the porosity of the hydrophobic material. Overall, the porosity of the membranes was all about 75.0%. It was the synergy of both addition of hPEA and the polymer concentration that makes the porosity stable. hPEA@PVDF membranes with higher polymer concentrations showed a larger thickness. Based on this, we assumed that the smaller pore sizes in hPEA@PVDF membranes would favor the adsorption capacity of the membranes due to the larger specific surface areas.

The internal morphology of hPEA@PVDF membranes was further investigated by WAXD analysis. The hPEA sample exhibited an amorphous peak at 17.9° in the WAXD spectra (Fig. S4†), while there existed a crystallization diffraction peak at 20.4° in hPEA@PVDF membranes and the pure PVDF membrane. This peak could be assigned to the characteristic β phase of PVDF.[44,45] The WAXD spectra showed that hPEA and PVDF were in separate phases in hPEA@PVDF membranes. Meanwhile, the intensity of the peak at 20.4° assigned to PVDF crystallization decreased with increasing content of hPEA, indicating that the strong interaction between hPEA and PVDF weakened the crystallization of PVDF. To further analyze the crystallization and melting behavior of hPEA@PVDF

membranes, differential scanning calorimeter (DSC) measurements were performed. As shown in Fig. 2, there was a melting peak of PVDF crystallization around 160 °C, and only one obvious glass transition temperature (T_g) of hPEA@PVDF membranes. The reason was that the T_g of pure PVDF (−38.9 °C) overlapped with that of hPEA (−36.2 °C), and it was difficult to distinguish their T_g, resulting in only one T_g in DSC curves. The melting temperature (T_m) and melting enthalpy (ΔH_m) of hPEA@PVDF membranes decreased slightly with increasing content of hPEA, which was in good agreement with WAXD results. These characterizations revealed that both hPEA and PVDF were in separate phases in hPEA@PVDF membranes.

Fig. 3 presents the XPS spectra of hPEA@PVDF membranes to evaluate the chemical composition of the surface. The pure PVDF membrane only showed peaks at 291 eV and 688 eV assigned to C and F, respectively, while various peaks corresponding to C (BE = 286 eV), N (BE = 400 eV), O (BE = 533 eV) and F (BE = 688 eV) signals were identified on the surface of the P10@hPEA3.3 sample. According to XPS measurements, the elemental mass concentrations of the surface can be calculated and marked in Fig. 3. The pure PVDF surface is comprised of 45.4 wt% C and 54.6% F, while the P10@hPEA3.3 surface contained 49.8 wt% C, 39.4 wt% F, 8.71 wt% O and 2.08 wt% N. The hPEA content on the membrane surface can be evaluated by the F/C ratio and the content of N atoms. It was understood that if we assume that the hPEA migrated to the interfaces of the membranes, the F/C ratio on the surface would be smaller than the theoretical F/C value based on the blend ratio in the feed. Indeed, the experimental mass concentration ratio of F to C in P10@hPEA3.3 was 0.791, smaller than the theoretical value 0.973. Moreover, the content of N atoms on the surface was much higher than the theoretical value of the blend ratio. These results revealed that amphiphilic hPEA was segregated and enriched onto the surface of hPEA@PVDF membranes during the phase inversion process to reduce the interfacial energy. The above analysis proved that hPEA wrapped on the surface of the PVDF skeleton to form a thin layer of hydrogel, a model for which is proposed in Scheme 1.

As an important parameter in filtration, the water flux was also enhanced by the improved hydrophilicity of hPEA@PVDF membranes. The minimum water flux of hPEA@PVDF membranes was 1.53 × 10^3 L m^{-2} h^{-1}, which was 40 times higher than that of the pure PVDF sample (38.2 L m^{-2} h^{-1}). The reason was that the amphiphilic hPEA layer on the PVDF skeleton enhanced the surface hydrophilicity of hPEA@PVDF membranes. The high water flux could favor fast and efficient filtration in the water treatment.

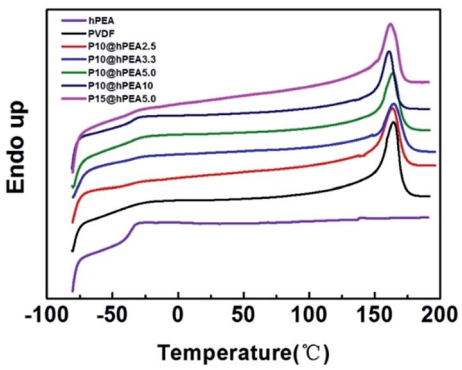

Fig. 2 DSC thermograms of hPEA@PVDF membranes. hPEA and PVDF were used as references. The scans were run at a heating rate of 20 °C min^{-1}.

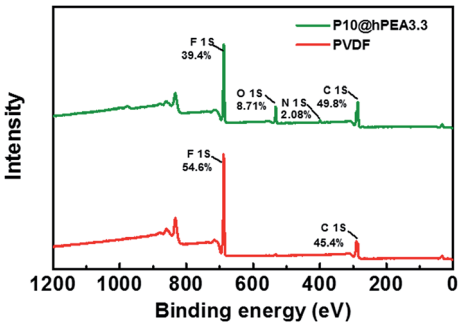

Fig. 3 XPS spectra of the pure PVDF and P10@hPEA3.3 membrane.

3.2 Selective adsorption of hydrophilic dyes

We then studied the adsorption behavior of the hPEA@PVDF porous membranes for twelve hydrophilic dyes. Seven fluorescein dyes were chosen because they have the same backbone and charge state in aqueous solution and are therefore helpful in elucidating the adsorption mechanism. Four azo dyes BBY, EVB, AR, and PS and the other dye MB were chosen because they are toxic and widely used in the dying industry. The experiment was conducted with initial concentrations of 15 μmol L^{-1} and 2.0 mg mL^{-1} for the dyes and hPEA@PVDF membranes, respectively. Taking ETB and MB as examples, it was observed that most of the ETB dye was adsorbed by the hPEA@PVDF membrane (Fig. 4a, inside picture); however, the MB dye still remained in the solution (Fig. 4b, inside picture). As shown in UV-vis spectra (Fig. 4), nearly 99% ETB was adsorbed by P15@hPEA5.0 after 48 h, but only 23% MB was adsorbed.

The saturated adsorption capacity (Q_{eq}), an important parameter for adsorbents in practical applications, was measured when the adsorptions reached equilibrium by analyzing the UV-vis spectra. The initial concentrations of the dyes and hPEA@PVDF membranes were fixed at 300 μmol L^{-1} and 1 mg mL^{-1}. Fig. 5 reveals that hPEA@PVDF membranes exhibited a high Q_{eq} for ETB, EB, TCF and RB. Nevertheless, hPEA@PVDF membranes showed a low Q_{eq} for Cal and MB. The large difference in Q_{eq} suggested the selective adsorption behavior of hPEA@PVDF membranes toward the hydrophilic dyes. Besides, the selective adsorption was regardless of charge states of both adsorbents and dyes, indicating that the interaction between the hPEA@PVDF membranes and dyes was independent of electrostatic interactions. Since pure PVDF could hardly adsorb the dyes (Fig. S7†), it could be concluded that hPEA played a critical role in hPEA@PVDF membranes for the selective adsorption of the dyes. To describe the relationship between the pore size and adsorption capacity, we

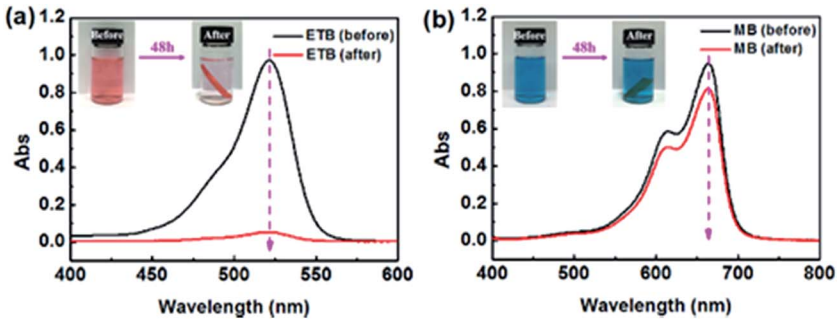

Fig. 4 Selective adsorption behaviors toward ETB and MB dyes: UV-vis spectra of ETB (a) and MB (b) before and after adsorption by P15@hPEA5.0 for 48 h. Insets are the photographs of ETB and MB solutions before and after adsorption (the concentration of dye solutions was 15 μmol L^{-1}, and the concentration of the hPEA@PVDF adsorbent was 2.0 mg mL^{-1}).

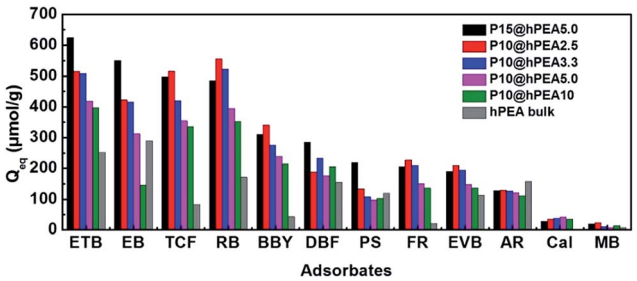

Fig. 5 Saturated adsorption capacities of hPEA in hPEA@PVDF membranes and hPEA bulk membranes (fluorescein dyes were dissolved in phosphate buffer (pH = 7.2), and azo dyes and MB were dissolved in deionized water). The concentration of the dye solution was 300 μmol L^{-1}, and the content of hPEA@PVDF adsorbents was 1 mg mL^{-1}; the adsorption time was 48 h).

compared the Q_{eq} of hPEA in the hPEA@PVDF porous membranes and hPEA bulk membrane. As shown in Fig. 5, hPEA@PVDF membranes with a smaller pore size possessed a larger Q_{eq}, and P15@hPEA5.0 with the smallest pores presented the largest adsorption capacity. Although the blend ratios of P15@hPEA5.0 and P10@hPEA3.3 were the same, P15@hPEA5.0 with a smaller pore size presented a larger Q_{eq}. It was assumed that the larger surface area derived from a smaller pore size promoted the adsorption capacity of the hPEA hydrogel layer. To further understand the relation between the porous structure and Q_{eq}, we measured the Q_{eq} of bulk hPEA without PVDF as reference. The Q_{eq} of P15@hPEA5.0 for ETB was 2.5 times higher than that of the hPEA bulk membrane. These results indicated that PVDF not only acted as the framework for hPEA, but also enhanced Q_{eq} because of its porous structure. Therefore, it was the synergy of both adsorption of hPEA and the porous structure of PVDF that contributed to the prominent adsorption performance of hPEA@PVDF membranes. The largest Q_{eq} for hPEA@PVDF porous membranes was 624 μmol g^{-1} (adsorbent: P15@hPEA5.0, dye: ETB), which was much higher than the largest Q_{eq} around 90 μmol g^{-1} for hPEA/PVA-IPN (adsorbent: hPEA/PVA-4/1, dye: ETB) in our previous studies.[40] The obvious increase of Q_{eq} proved the excellent adsorption ability of hPEA@PVDF membranes compared with other materials.

The adsorption kinetics of twelve dyes were investigated to understand the interaction mechanism between hPEA@PVDF membranes and dyes (Fig. 6). Here, P15@hPEA5.0 was chosen as the representative membrane because of its large Q_{eq}. The adsorption capacities for the dyes with high Q_{eq} (such as ETB, EB and RB) increased rapidly at first, and then continued to increase at a relatively slow rate. In contrast, the dyes with low Q_{eq} (such as MB and Cal) presented low adsorption capacities and adsorption rates. Huge differences of adsorption capacities and adsorption rates existed among dyes regardless of their charge states. The result further confirmed that the interaction mechanism between hPEA@PVDF membranes and dyes was not the electrostatic interaction. The pseudo-second-order kinetic model (Fig. S8 and Table S2†) was adopted to examine the adsorption mechanism. The R^2 values (Table S2†) obtained from the pseudo-second-order model were all nearly 1. Besides, the calculated amount of dye adsorption at equilibrium was in agreement with the experimental amount of dye adsorbed at equilibrium (Q_{eq}), suggesting that the pseudo-second-order model fits well with the adsorption data. The higher values of k and Q_{eq} meant a stronger affinity between hPEA@PVDF membranes and dyes. The differences of k and Q_{eq} both revealed the selective adsorption behavior of hPEA@PVDF membranes toward hydrophilic dyes.

We conducted the adsorption isotherm study for dyes ETB, EB and Cal onto the P15@hPEA5.0 membrane to understand how hybrid hydrogels and the hydrophilic dyes interacted with each other and estimated the characteristics of the adsorption system. The equilibrium adsorption data were analyzed by using the Langmuir and Freundlich isotherm models (Fig. S9 and Table S3†). We found that the Langmuir model was suitable for describing the adsorption equilibrium of ETB and EB, and the adsorption of Cal followed the Freundlich model. Therefore, chemisorption is dominant in the adsorption of ETB and EB with a strong affinity onto the hPEA@PVDF membrane from isotherms studies.

3.3 Separation of dyes by molecular filtration

Motivated by the unique selective adsorption, porous structure and high adsorption capacity, the hPEA@PVDF membranes can be extended to practical separation through molecular

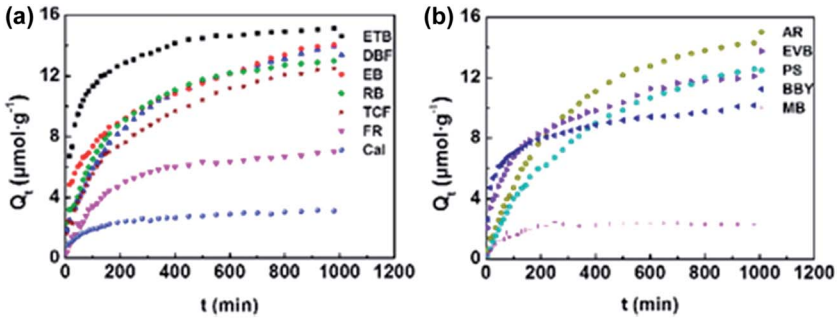

Fig. 6 Adsorption kinetics of twelve dyes by P15@hPEA5.0 membranes at 25 °C: (a) adsorption capacity Q_t *versus* time for the adsorption of fluorescein dyes; (b) adsorption capacity Q_t *versus* time for the adsorption of azo dyes and MB (15 mL dye solution with a concentration of 40 μmol L^{-1}; adsorbent 30 mg).

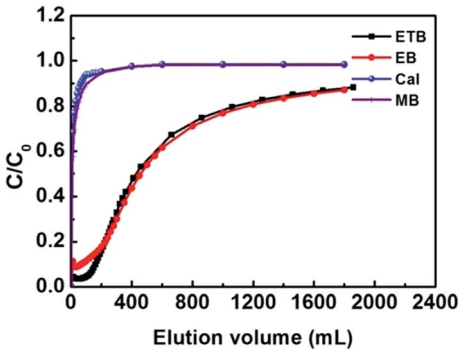

Fig. 7 Breakthrough curves of ETB, EB, MB and Cal solutions through the P15@hPEA5.0 membrane (dye solution with an initial concentration of 40 μmol L^{-1}; the size and mass of the membrane were about 4 cm in diameter and 110 mg, respectively; pH = 7.2).

filtration. Breakthrough curves of four dyes ETB, EB, MB and Cal through the P15@hPEA5.0 membrane were obtained in advance by determining the flow-through outlet concentration. The concentration of the dyes was 40 μmol L^{-1} in the feed, and the mass of P15@hPEA5.0 was 110 mg. As shown in Fig. 7, the concentrations of MB and Cal in filtrates reached the feed concentration after 400 mL elution volume, while the concentrations of ETB and EB were only half of the feed concentrations. Besides, the concentrations of ETB and EB still hadn't reached the filtration stage when the volume of feed solutions was 1800 mL. These results indicated that hPEA@PVDF membranes could remove ETB and EB from aqueous solutions effectively, but could not capture MB and Cal. The selective filtration performance coincided with the adsorption behavior and adsorption kinetics results, which should be ascribed to the selective adsorption behavior of hPEA@PVDF membranes toward dyes.

Based on the selective adsorption behavior of hPEA@PVDF membranes *via* filtration, dye separation tests were carried out to attest that hPEA@PVDF membranes could adsorb dyes selectively from mixed dye solutions through molecular filtration. Using P15@hPEA5.0 as the filter membrane, two dye mixtures of ETB/MB and RB/Cal were separated by filtration. 100 mL of a mixture of dye solution was forced to flow through the P15@hPEA5.0 membrane at a flow rate of 6.7 mL min^{-1}, and the

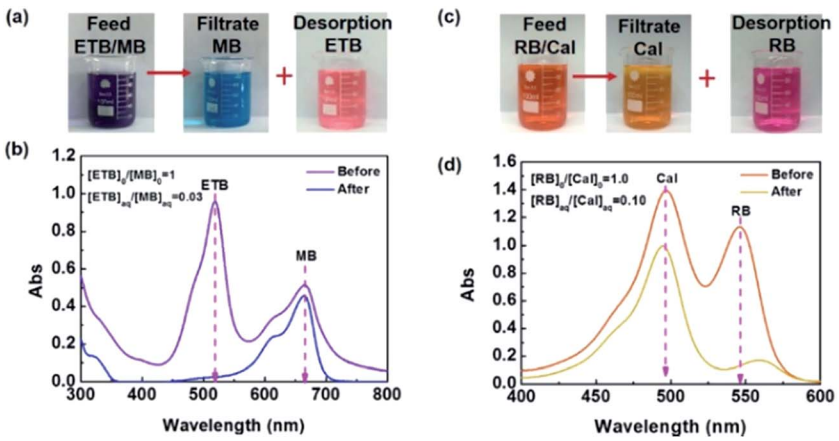

Fig. 8 Filtration of dye mixtures of ETB/MB and ETB/Cal through P15@hPEA5.0 (pH = 7.2). Photographs of ETB/MB (a) and RB/Cal (c) before and after filtration as well as the photographs after desorption. UV-vis spectra of the ETB/MB (b) and ETB/Cal (d) mixture before and after filtration (the initial concentration of the dyes was 20 μmol L^{-1}; the size and mass of the membrane were about 4 cm in diameter and 110 mg, respectively; the flow rate was 6.67 mL min^{-1}).

initial concentration ratios of both ETB/MB and RB/Cal were 1.0. As shown in Fig. 8, the color of the ETB/MB solution changed from purple to blue after filtration, suggesting that ETB was captured by the P15@hPEA5.0 membrane, but MB was left in the filtrate (Fig. S10 and Movie S1†). The concentrations of ETB and MB in the filtrate were determined by UV-vis spectra. As shown in Fig. 8b, the concentration ratio of ETB to MB was 0.03. In other words, the purity of MB in the filtrate was about 97% after filtration. The mixture solution of RB/Cal was also separated through the same method. As shown in Fig. 8c, the orange feed solution turned yellow after filtration, suggesting that most of the RB was adsorbed by the P15@hPEA5.0 membrane. The concentration ratio of RB to Cal in the solution decreased from 1.0 to 0.1 (Fig. 8d), also indicating that RB with a higher Q_{eq} and faster adsorption rate was separated from the mixture.

As the practical dye-polluted water usually contains a mixture of several dyes, we also conducted filtration experiments of the solution with four kinds of dyes by using P15@hPEA5.0 as the filter membrane. In the mixture of dye solution, ETB, EB and RB with the high Q_{eq} were expected to be captured by P15@hPEA5.0, while Cal would be left in the filtrate. As shown in Fig. 9, the color of the solution changed from orange to yellow after the first filtration, which was close to the color of the Cal solution. After filtration for the second time, the color of the filtrate turned light yellow, and UV-vis spectra revealed that almost all ETB, EB and RB were removed by filtration, while Cal was still in the filtrate.

3.4 Regeneration

Finally, the regenerative capacity of the hPEA@PVDF membranes was evaluated. Taking the ETB/MB adsorption experiment as the example, the P15@hPEA5.0 membrane adsorbing ETB was regenerated using NaOH aqueous solution with similar filtration equipment. After 5 adsorption–washing tests, the P15@hPEA5.0 membrane could still separate the mixture with high efficiency, and the purity of MB in the filtrate was over 87% even in the 5th cycle (Fig. 10a). The cross sectional images after the 5th regeneration process showed that the porous structure is maintained (Fig. 10b), and the magnified cross sectional morphologies from the bottom side showed the original sponge structure (Fig. 10c). The good stability of hPEA@PVDF membranes might be ascribed to the cross-linked structure of hPEA and excellent mechanical and chemical-resistant performance of the PVDF skeleton. These experimental results verified that hPEA@PVDF membranes exhibited great regeneration performance and thus they will have great potential in the field of water treatment.

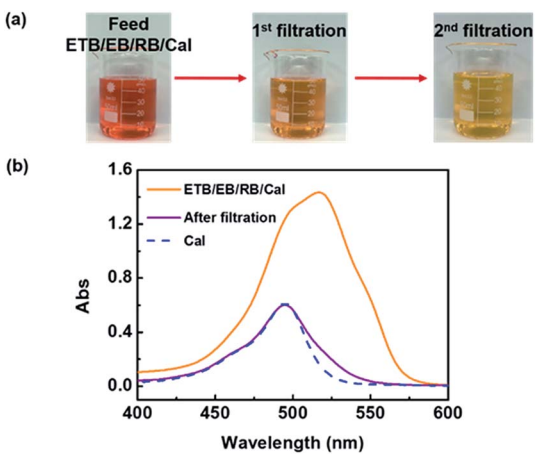

Fig. 9 Filtration of the dye mixture through P15@hPEA5.0 (pH = 7.2): (a) photographs of ETB/EB/RB/Cal before filtration, after the 1st and the 2nd filtration (b) UV-vis spectra of the solution before the filtration and after the 2nd filtration (the initial concentration of the dyes was 10 μmol L^{-1}; the size and mass of the membrane were about 4 cm in diameter and 110 mg, respectively; the flow rate was 6.67 mL min^{-1}).

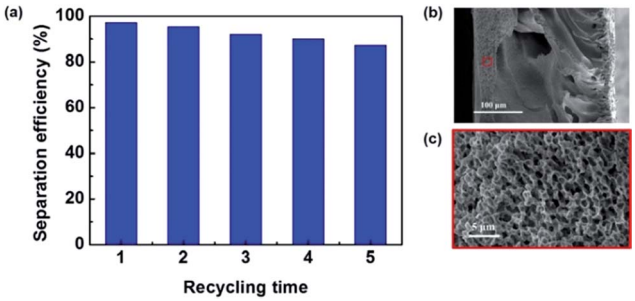

Fig. 10 Regeneration test for the P15@hPEA5.0 membrane: (a) separation efficiency of the regenerated P15@hPEA5.0 membrane at different recycling times. (b) SEM cross-sectional image of the P15@hPEA5.0 membrane after cycling 5 times. (c) Magnified cross-sectional image from the bottom side of the P15@hPEA5.0 membrane after cycling 5 times.

4. Conclusion

In summary, we demonstrated a novel kind of hPEA@PVDF porous membrane through non-solvent induced phase separation, in which the porous skeleton of PVDF was covered by the cross-linked layer of hPEA hydrogel. The porous skeleton of PVDF provided a mechanically and chemically stable support for the hPEA hydrogel, while the cross-linked layer of hPEA hydrogel could offer selective adsorption capacity to hPEA@PVDF membranes for the removal of dyes and enhance the hydrophilicity of the PVDF porous skeleton. Regardless of their charge states, hPEA@PVDF porous membranes exhibited quick adsorption behavior toward ETB, RB and EB with a large Q_{eq}, but very slow adsorption behavior toward Cal and MB with a low Q_{eq}. Based on the unique selective adsorption behavior toward hydrophilic dyes and the porous structure, hPEA@PVDF membranes could separate mixtures of dyes in aqueous solution through molecular filtration with a high flux. The integration of fast separation, easy regeneration and low cost makes hPEA@PVDF porous membranes suitable for potential applications such as separation and water treatment.

Acknowledgements

The authors thank the National Nature Science Foundation of China (21522403, 51373098), the National Basic Research

Program (2013CB834506) and the Education Commission of Shanghai Municipal Government (15SG13) for their financial support.

References

1 M. H. Sun, S. Z. Huang, L. H. Chen, Y. Li, X. Y. Yang, Z. Y. Yuan and B. L. Su, *Chem. Soc. Rev.*, 2016, **45**, 3479–3563.
2 I. Soroko, Y. Bhole and A. G. Livingston, *Green Chem.*, 2011, **13**, 162–168.
3 P. Vandezande, L. E. M. Gevers and I. F. J. Vankelecom, *Chem. Soc. Rev.*, 2008, **37**, 365–405.
4 A. W. Zularisam, A. F. Ismail and R. Salim, *Desalination*, 2006, **194**, 211–231.
5 X. Gao, L. P. Xu, Z. Xue, L. Feng, J. Peng, Y. Wen, S. Wang and X. Zhang, *Adv. Mater.*, 2014, **26**, 1771–1775.
6 M. Tao, L. Xue, F. Liu and L. Jiang, *Adv. Mater.*, 2014, **26**, 2943–2948.
7 T. A. Saleh, A. Sarı and M. Tuzen, *Chem. Eng. J.*, 2017, **307**, 230–238.
8 V. O. Shikuku, C. O. Kowenje and W. N. Nyairo, Fundamentals and sources of magnetic nanocomposites and their sorption properties, in *Advanced Nanomaterials for Water Engineering, Treatment and Hydraulics*, ed. Tawfik A. Saleh, IGI Global Publishers, 2017, ISBN: 9781522521365.
9 D. E. Jiang, V. R. Cooper and S. Dai, *Nano Lett.*, 2009, **9**, 4019–4024.
10 C. H. Lau, K. Konstas, A. W. Thornton, A. C. Y. Liu, S. Mudie, D. F. Kennedy, S. C. Howard, A. J. Hill and M. R. Hill, *Angew. Chem., Int. Ed.*, 2015, **54**, 2669–2673.
11 B. S. Ghanem, R. Swaidan, E. Litwiller and I. Pinnau, *Adv. Mater.*, 2014, **26**, 3688–3692.
12 S. B. Lee, D. T. Mitchell, L. Trofin, T. K. Nevanen, H. Söderlund and C. R. Martin, *Science*, 2002, **296**, 2198–2200.
13 T. A. Saleh, M. M. Al-Shalalfeh and A. A. Al-Saadi, *Sci. Rep.*, 2016, **6**, 32185.
14 N. B. McKeown and P. M. Budd, *Chem. Soc. Rev.*, 2006, **35**, 675–683.
15 A. A. Alturki, N. Tadkaew, J. A. McDonald, S. J. Khan, W. E. Price and L. D. Nghiem, *J. Membr. Sci.*, 2010, **365**, 206–215.
16 T. A. Saleh and V. K. Gupta, *Sep. Purif. Technol.*, 2012, **89**, 245–251.
17 H. B. Park, C. H. Jung, Y. M. Lee, A. J. Hill, S. J. Pas, S. T. Mudie, E. Van Wagner, B. D. Freeman and D. J. Cookson, *Science*, 2007, **318**, 254–258.
18 D. L. Gin and R. D. Noble, *Science*, 2011, **332**, 674–676.
19 J. Shang, G. Li, R. Singh, Q. Gu, K. M. Nairn, T. J. Bastow, N. Medhekar, C. M. Doherty, A. J. Hill, J. Z. Liu and P. A. Webley, *J. Am. Chem. Soc.*, 2012, **134**, 19246–19253.
20 B. J. Hinds, N. Chopra, T. Rantell, R. Andrews, V. Gavalas and L. G. Bachas, *Science*, 2004, **303**, 62–65.
21 M. Khayet, C. Y. Feng, K. C. Khulbe and T. Matsuura, *Polymer*, 2002, **43**, 3879–3890.
22 T. Xiao, P. Wang, X. Yang, X. Cai and J. Lu, *J. Membr. Sci.*, 2015, **489**, 160–174.
23 F. Liu, N. A. Hashim, Y. Liu, M. R. M. Abed and K. Li, *J. Membr. Sci.*, 2011, **375**, 1–27.
24 H. H. Park, B. R. Deshwal, H. D. Jo, W. K. Choi, I. W. Kim and H. K. Lee, *Desalination*, 2009, **243**, 52–64.
25 Y. Xiao, X. D. Liu, D. X. Wang, Y. K. Lin, Y. P. Han and X. L. Wang, *Desalination*, 2013, **311**, 16–23.
26 C. Park, S. W. Hong, T. H. Chung and Y. S. Choi, *Desalination*, 2010, **250**, 673–676.
27 X. S. Yi, S. L. Yu, W. X. Shi, N. Sun, L. M. Jin, S. Wang, B. Zhang, C. Ma and L. P. Sun, *Desalination*, 2011, **281**, 179–184.
28 B. Wang, J. Ji and K. Li, *Nat. Commun.*, 2016, **7**, 12804.
29 S. Boributh, A. Chanachai and R. Jiraratananon, *J. Membr. Sci.*, 2009, **342**, 97–104.
30 W. Zhang, Y. Zhu, X. Liu, D. Wang, J. Li, L. Jiang and J. Jin, *Angew. Chem.*, 2014, **126**, 875–879.
31 T. A. Saleh and V. K. Gupta, *Nanomaterial and Polymer Membranes, Synthesis, Characterization, and Applications*, Elsevier, 2016, ISBN13: 9780128047033.
32 N. Chen and L. Hong, *Polymer*, 2002, **43**, 1429–1436.
33 W. Z. Lang, Z. L. Xu, H. Yang and W. Tong, *J. Membr. Sci.*, 2007, **288**, 123–131.
34 J. F. Hester, P. Banerjee and A. M. Mayes, *Macromolecules*, 1999, **32**, 1643–1650.
35 Y. H. Zhao, B. K. Zhu, L. Kong and Y. Y. Xu, *Langmuir*, 2007, **23**, 5779–5786.
36 F. Liu, Y. Y. Xu, B. K. Zhu, F. Zhang and L. P. Zhu, *J. Membr. Sci.*, 2009, **345**, 331–339.
37 X. Lü, X. Wang, L. Guo, Q. Zhang, X. Guo and L. Li, *J. Membr. Sci.*, 2016, **520**, 933–940.
38 T. Rajasekhar, M. Trinadh, P. Veera Babu, A. V. S. Sainath and A. V. R. Reddy, *J. Membr. Sci.*, 2015, **481**, 82–93.
39 R. Wang, B. Yu, X. Jiang and J. Yin, *Adv. Funct. Mater.*, 2012, **22**, 2606–2616.
40 P. Zhang, J. Yin and X. Jiang, *Langmuir*, 2014, **30**, 14597–14605.
41 S. Deng, H. Xu, X. Jiang and J. Yin, *Macromolecules*, 2013, **46**, 2399–2406.
42 M. S. Khehra, H. S. Saini, D. K. Sharma, B. S. Chadha and S. S. Chimni, *Dyes Pigm.*, 2006, **70**, 1–7.
43 M. Chethana, L. G. Sorokhaibam, V. M. Bhandari, S. Raja and V. V. Ranade, *ACS Sustainable Chem. Eng.*, 2016, **4**, 2495–2507.
44 S. Yu, W. Zheng, W. Yu, Y. Zhang, Q. Jiang and Z. Zhao, *Macromolecules*, 2009, **42**, 8870–8874.
45 M. C. Branciforti, V. Sencadas, S. Lanceros-Mendez and R. Gregorio, *J. Polym. Sci., Part B: Polym. Phys.*, 2007, **45**, 2793–2801.